Reassessing the age of Karpathos ophiolite (Dodecanese, Greece): consequences for Aegean correlations and Neotethys evolution

Fabrice Cordey, Frédéric Quillévéré

Title page

Title: Reassessing the age of Karpathos ophiolite (Dodecanese, Greece): consequences for Aegean correlations and Neotethys evolution.

Category: Original Article

Authors : FABRICE CORDEY, FRÉDÉRIC QUILLÉVÉRÉ

Université de Lyon, Université Claude Bernard Lyon 1, Laboratoire de Géologie de Lyon Terre Planètes Environnement LGLTPE, CNRS-UMR 5276, Bd du 11 Novembre 1918, 69622 Villeurbanne, France

Short title: Age of Karpathos ophiolite

Corresponding author: fabrice.cordey@univ-lyon1.fr

Abstract

While the Neogene history of the Eastern Mediterranean region is now fairly well understood, our knowledge of older regional paleogeographies is less accurate, especially the positions of blocks and nappes constituting the Aegean Islands prior to the Cenozoic. Our study focuses on the ophiolite exposed on the island of Karpathos (Dodecanese), which is located in the Aegean fore-arc at a pivotal position between the 'western' and 'eastern' ophiolites of the Mediterranean region and where conflicting Late Jurassic and Late Cretaceous ages have led to diverging tectonic and paleogeographic interpretations. To test these ages, we targeted the radiolarian cherts that depositionally overlie the ophiolite and extracted diagnostic radiolarian assemblages of Aptian (~125–113 Ma), early-middle Albian (~113–105 Ma), and Turonian (~93.9–89.8 Ma) ages. These results suggest that previous Late Cretaceous K-Ar isotopic ages (from 95.3 ± 4.2 Ma to 81.2 ± 1.6 Ma) may have been reset by Late Cretaceous metamorphism or affected by argon loss. Overall, the new Early Cretaceous ages show that the Karpathos ophiolite should not be correlated with the Pindos Nappes of Greece or the ophiolites of Cyprus or Syria but rather with the Lycian Nappes of Turkey and their root located in the Izmir−Ankara−Erzincan Suture Zone. Therefore, the Karpathos ophiolite represents a remnant of the Northern Neotethys, not the Pindos Ocean or the proto-Eastern Mediterranean Basin.

Keywords: ophiolite, radiolarite, Radiolaria, Cretaceous, Karpathos, Aegean fore-arc, Neotethys.

1. Introduction

Present-day convergent margins are often characterized by the occurrence of ophiolites along the upper plate(s) in a large variety of settings related to terrane accretion processes (see Dilek & Furnes, 2014, and references therein). This study focuses on the island of Karpathos (Dodecanese, Greece), which belongs to the Aegean fore-arc (Figure 1) and is located at the junction between two important ophiolite domains of the Mediterranean region: the western region (Dinarides, Hellenides) and the eastern region (Taurides, Cyprus, Syria) (Robertson, 2002). Although the Neogene history of the Eastern Mediterranean region is fairly well understood following a very large number of studies and the application of powerful tools such as high-resolution seismic tomography (Royden & Faccenna, 2018, and references therein), our knowledge of older regional paleogeographies is less accurate. In the Aegean Sea, the origin of scattered blocks and nappes constituting the Cyclades, Crete and the Dodecanese is not well understood. In particular, there are some difficulties in establishing precise geological correlations between these islands and the surrounding continental margins (Roche *et al.* 2018).

Due to its "pivotal" position between the ophiolite regions of Greece and Turkey, Karpathos has attracted significant geological attention for more than a century (see Appendix "Pioneering studies on Karpathos", online Supplementary Material at http://journals.cambridge.org/geo), but diverging interpretations about the age of the ophiolite have led to conflicting views: while K-Ar geochronology documented Late Cretaceous isotopic ages (Koepke, Kreuzer & Seidel, 1985; Hatzipanagiotou, 1991; Koepke, Seidel & Kreuzer, 2002), the sedimentary rocks overlying the ophiolite were considered to be early Early Cretaceous based on calpionellids, suggesting that the ophiolite could be as old as Late Jurassic (Davidson-Monett, 1974; Aubouin, Bonneau & Davidson, 1976). These two distinct ages led to very different paleogeographic scenarios: the Karpathos ophiolite has been

interpreted as a remnant of the Pindos Ocean (Aubouin, Bonneau & Davidson, 1976), the Northern Neotethys (Robertson, 2002), or the Southern Neotethys due to age and petrological affinities with Late Cretaceous ophiolites of Turkey, Syria and Oman (Koepke, Seidel & Kreuzer, 2002).

Since no modern radiolarian study has ever been undertaken on the island, we have revisited Karpathos and reassessed the potential of its supra-ophiolitic sedimentary strata, with three major objectives: 1) to solve this chronological conundrum by focusing on radiolarian cherts, 2) to improve the correlations between Karpathos and the surrounding Mediterranean ophiolites (Greece, Crete, Rhodes, Turkey), and 3) to develop a better understanding of Neotethys paleogeography and tectonics in the Aegean region.

2. Geological setting

2.a. The Xindothio Unit

The Karpathos ophiolite forms relatively small exposures (Figure 2a–c) of mainly serpentinized peridotite with minor occurrences of gabbro and dolerite dykes ('dismembered' type after Coleman, 1977). Early geological studies provided some preliminary descriptions of the magmatic rocks and associated sedimentary strata (de Stefani, Forsyth Major & Barbey, 1895; Martelli, 1916; Christodoulou 1960; Aubouin & Dercourt, 1970; online Supplementary Material at http://journals.cambridge.org/geo). Later, geological mapping demonstrated that these rocks lie within tectonic slices at the top of the nappe pile exposed in the central part of the island and belong to a tectono-stratigraphic succession described as the 'Xindothio Unit' (Davidson-Monett, 1974; Aubouin, Bonneau & Davidson, 1976; Hatzipanagiotou, 1987). The Xindothio Unit overlies the Kalilimni Unit, a Jurassic to Eocene parautochthonous carbonate platform (Figure 2a), and comprises eight subunits from base to top (Figure 3a): ammonite-bearing marl, belemnites-bearing sandstone, platy limestone with filaments (*Halobia*), grey

platy limestone, mafic and ultramafic rocks (serpentinite, gabbro, dolerite), red radiolarite and pink microcrystalline limestone, platy green limestone, fine-grained limestone and siliceous beds. The base of the Xindothio Unit has been dated as early Late Triassic (Carnian) with ammonites (*Tropites subbullatus*; Aubouin, Bonneau & Davidson, 1976), while the top is Campanian–Maastrichtian based on planktonic foraminifera (*Globotruncana stuarti, G. stuartiformis,* and *G. contusa*; Aubouin, Bonneau & Davidson, 1976).

Mafic and ultramafic rocks are commonly found in tectonic contact with the underlying units, whereas the radiolarites depositionally overlie the ophiolite at many locations in the Lastos and Menetes areas (Davidson-Monett, 1974; Aubouin, Bonneau & Davidson, 1976; Hatzipanagiotou, 1987, 1988) (Figures 2a–c, 3a). The depositional nature of this contact is supported by good lateral continuity of the radiolarites which show no significant deformation. The rarity of basalts and the direct contact between the magmatic rocks and the radiolarites suggest that the Karpathos ophiolite formed by relatively slow spreading. Near the contact, red chert beds are 5-15 cm thick, whereas these beds are less abundant upsection and crop out as thin continuous layers or chert nodules. Overall, the radiolarite-pink limestone subunit is approximately 40 m thick (Figures 3a, 4).

2.b. Previous ages of the ophiolite and overlying strata

Vinassa de Regny (1901) provided the first study of Karpathos radiolarians, which he observed within ‘phtanites’ (black cherts) and ‘argillaceous jaspers’ (red-maroon cherts) collected in the Lastos area (Figure 2a, b). This pioneering work led to the description of fifty-eight radiolarian morphotypes (online Supplementary Material at http://journals.cambridge.org/geo), although most of the identified genera are now classified as *nomen dubium* (O’Dogherty *et al.* 2009). In the light of current radiolarian taxonomy, some of the forms illustrated by Vinassa de Regny (1901) resemble the modern genera *Archaeospongoprunum*, *Hiscocapsa*, *Paronaella*, *Pseudoeucyrtis*, *Pseudodictyomitra*, and

Triactoma, but their occurrence is difficult to confirm given the discrepancies between 1900s drawings and present-day taxonomy based on three-dimensional scanning electron microscope (SEM) observations. Vinassa de Regny (1901) suggested that the faunal assemblage was possibly Late Cretaceous, although this age determination was tentative due to the absence of radiolarian biozonation at the time. Later, an age determination was obtained on the radiolarite-pink limestone subunit with one calpionellid assemblage (Davidson-Monett, 1974; Aubouin, Bonneau & Davidson, 1976) and was assigned to the middle−late Berriasian (145−139.8 Ma; Cohen *et al.* 2013, updated 2018). Consequently, these authors suggested that the ophiolite could be as old as Late Jurassic.

The K-Ar isotopic ages obtained later on the magmatic rocks (hornblende grains extracted from intrusive dolerites) are much younger than the overlying sedimentary strata (Table 1; Koepke, Kreuzer & Seidel, 1985; Hatzipanagiotou, 1991; Koepke, Seidel & Kreuzer, 2002). In Lastos, two ages range between 84.7 and 79.6 Ma, encompassing the middle Santonian−middle Campanian interval (Cohen *et al.* 2013, updated 2018). In Menetes, the isotopic ages range between 99.5 and 88.4 Ma, corresponding to the middle Cenomanian−middle Coniacian interval.

3. Studied sections and methods

Our study focused on identifying the contact between mafic/ultramafic rocks and the overlying radiolarian cherts in order to select a few localities for sampling. This contact is exposed in the high valley of Lastos on the eastern flank of Mount Kalilimni (Figures 2b, 5) and near the village of Menetes on the southern flank of Mount Homali (Figure 2c). To maximize the quality of the faunas, we selected a variety of radiolarian samples in accordance

147 with specific field techniques previously applied to suture zones and fore-arc belts (Cordey &
148 Krauss, 1990; Cordey & Cornée, 2009). Radiolarians were then extracted by repetitive
149 leaching of samples with low-concentration hydrofluoric acid (HF) and then hand-picked and
150 mounted on aluminium stubs for SEM observation and taxonomical identifications (Tabletop
151 SEM Phenom ProX, University of Lyon).
152
153 In Lastos, our samples were collected from two sections:
154 1/ section 'North Lastos road' (Figure 2b; Table 2). This section is composed of an outcrop of
155 serpentinites depositionally overlain by radiolarian cherts and pink limestones. KAL01 was
156 collected from a red radiolarite bed situated 30 cm above the serpentinite body (Figure 3b).
157 Similar stratigraphic contacts between serpentinites and radiolarites are visible at several
158 locations along the North Lastos road (Figures 2b, 5b, c).
159 2/ section 'Hill 730 m' (Figure 2b, Table 2). This section was previously described by
160 Davidson-Monett (1974) and Aubouin, Bonneau & Davidson (1976) under the name 'section
161 of hill 738 m' (Figures 3b, 4) and renamed to follow the revised topography available on the
162 Karpathos-Kasos map sheet (Psimenos *et al.* 2017). Sample KAL02 is from a bed of red
163 radiolarian chert at the base of the radiolarite-pink limestone subunit located just above the
164 contact with gabbros and serpentinites (Figures 3b, 5a, 5e). Sample KAL03 is from a red
165 nodular radiolarian chert bed and was collected at the top of the radiolarite-pink limestone
166 subunit (Figures 3b, 5d).
167
168 Near Menetes, our sample locality KAM01 (Figure 2c, Table 2) is from a bed of radiolarite
169 interbedded with pink limestones, 150 m to the south of a well-exposed serpentinite outcrop at
170 the foot of Mount Homali (Figure 3b).
171
172 **4. Results**

The preservation of radiolarians extracted from our chert samples varies from moderate to good at both the Lastos and Menetes locations. All of the radiolarian taxa and assemblages identified in the samples are listed in Table 3. Morphotypes with biochronological significance are illustrated in Figure 6.

KAL01 comprises sixteen identified taxa (Table 3). Among them, an assemblage composed of *Archaeodictyomitra gracilis*, *Crucella euganea*, *Crucella messinae*, *Hiscocapsa asseni*, *Hiscocapsa grutterinki* and *Pseudodictyomitra lodogaensis* corresponds to the unitary associations zones (UAZ) 4–9 of O'Dogherty (1994) of early-late Aptian age. Other Early Cretaceous species include *Cenodiscaella sphaeroconus*, *Homoeoparonaella* sp. cf. *speciosa*, *Mesosaturnalis* sp., *Paronaella* sp., *Pseudocrucella* sp. aff. *kubischa*, *Pseudoeucyrtis*(?) *fusus*, *Stichomitra communis*, *Ultranapora* sp. cf. *durhami* and *Xitus* sp. aff. *spicularius.* Among them, *Stichomitra communis* is known from the Aptian−Turonian interval (UAZ 42–46; Goričan, 1994). We interpret the morphotype illustrated in Figure 6 (n° 14) as *Dictyomitra montisserei*, which we consider to have a slightly longer age range than previously proposed (UAZ 10–20 of Albian−Turonian age; O'Dogherty, 1994).

KAL02 is composed of eight radiolarian taxa (Table 3). The co-occurrence of *Crucella messinae*, *Cyclastrum satoi*, *Dactyliosphaera lepta*, *Hexapyramis* sp. cf. *precedis*, *Mesosaturnalis levis* and *Xitus spicularius* points to UAZ 11–12 of early–middle Albian age (O'Dogherty, 1994). Some other taxa have longer age ranges, such as *Alievium* sp. (Bajocian–Maastrichtian, O'Dogherty *et al.* 2009) and *Obeliscoites* sp. cf. *perspicuus* (UAZ 1–19, Barremian–Cenomanian; O'Dogherty, 1994).

KAL03 comprises ten radiolarian taxa (Table 3). *Alievum* sp. cf. *superbum*, *Crucella cachensis*, and *Dictyomitra napaensis* are known as Turonian (Pessagno, 1976). Other taxa have been found to co-occur in Turonian biozones, such as *Stichomitra communis* (UAZ 42–48 of late Aptian–Turonian; Goričan, 1994), *Dictyomitra montisserei* (UAZ 10–20, Albian–Turonian; O'Dogherty, 1994), *Pseudodictyomitra pseudomacrocephala* (UAZ 10–21, Albian–Turonian; O'Dogherty, 1994), and *Afens* sp. (Turonian–Campanian; O'Dogherty *et al.* 2009).

KAM01 contains seven radiolarian taxa, including species reported from the biozonation of O'Dogherty (1994), such as *Distylocapsa micropora* (UAZ 10–18) and *Thanarla brouweri* (UAZ 1–12), corresponding to a middle Albian age. Other taxa are *Archaeospongoprunum renaensis* (Albian; Pessagno, 1977), *Cenodiscaella tuberculatum* (early Cenomanian–?early Turonian; Pessagno, 1977), *Staurosphaeretta* sp. (late Aptian–early Turonian; O'Dogherty *et al.* 2009), *Pseudodictyomitra lodogaensis* (UAZ 42–46, late Aptian–late Albian; Goričan, 1994), and *Triactoma* sp. (early Pliensbachian–late Turonian; O'Dogherty *et al.* 2009).

In summary, the radiolarian ages established for the radiolarite-pink limestone subunit of the Xindothio Unit are from base to top: early–late Aptian (KAL01; ~125–113 Ma; Cohen *et al.* 2013, updated 2018), early–middle Albian (KAL02; ~113–105 Ma), middle Albian (KAM01; ~110–105 Ma), and Turonian (KAL03; ~93.9–89.8 Ma) (Figure 3a, b).

5. Discussion

5.a. Comparison with previous microfossil ages

The three Aptian and Albian radiolarian ages (~125–105 Ma) obtained at the base of the radiolarite-pink limestone subunit at Lastos (KAL01, KAL02) and Menetes (KAM01) are significantly younger than the Berriasian age (145–139.8 Ma) previously reported from the same sequence (Davidson-Monett, 1974; Aubouin, Bonneau & Davidson, 1976). A similar issue applied on Rhodes, where Danelian *et al.* (2001) established that Berriasian calpionellids from the Profitis Ilias succession had been misidentified. This situation could also be the case in Karpathos. Another hypothesis is that these calpionellids have been reworked. In any case, based on results obtained in three sections in two separate areas (Lastos and Menetes; Figure 3a, b), our data show that the radiolarites of the Xindothio Unit are not Berriasian but rather Aptian–Albian.

Our younger radiolarian assemblage is Turonian (~93.9–89.8 Ma) and was obtained at the top of the radiolarite-pink limestone subunit (KAL03). Foraminifera of similar age were reported from the base of the platy limestone subunit (Davidson-Monett, 1974; Aubouin, Bonneau & Davidson, 1976).

5.b. Comparison with K-Ar isotopic ages

K-Ar isotopic ages of Koepke, Seidel, & Kreuzer (2002) are shown in Table 1. At Menetes, the age difference with the radiolarian data is minor, as the oldest isotopic age of 95.3 ± 4.2 Ma fits into the early Cenomanian (Cohen *et al.* 2013, updated 2018). At Lastos, the age difference is greater: while radiolarians near the contact are Aptian, the oldest isotopic age is middle Santonian (84.7 Ma, Table 1). To explain such a discrepancy, four hypotheses are considered below:

1/ Aptian–Albian radiolarians were reworked and redeposited in younger Late Cretaceous sediments. This process seems unlikely since the radiolarian assemblages do not show any unusual mixing of incompatible taxa (Table 3). These assemblages also document a coherent

succession of upward-younging ages (Aptian > early–middle Albian > middle Albian > Turonian; Figure 3a). In addition, the Turonian ages obtained independently with planktonic foraminifera (Aubouin, Bonneau & Davidson, 1976) and radiolarians (this study) near the contact between radiolarite-pink limestone and platy limestone subunits are both older than the K-Ar isotopic ages of Koepke, Seidel, & Kreuzer (2002).

2/ The contact between mafic/ultramafic rocks and radiolarites is tectonic. However, this hypothesis is not consistent with our field observations or those of Davidson-Monett (1974), Aubouin, Bonneau & Davidson (1976) and Hatzipanagiotou (1988). The Xindothio Unit is not an accretionary-type "broken formation" where subunits are chaotically juxtaposed. Instead, it shows good reproducibility of the stratigraphic contact between the magmatic rocks and the overlying radiolarian cherts, not only at Lastos but also at Menetes (Figure 2b, c). In addition, there is good lateral continuity of the contact as shown by the parallel bedding of the radiolarite-pink limestone subunit along strike (Figure 5b, c). One could argue that the Karpathos ophiolite is dismembered and that mafic and ultramafic rocks may not be of the same age as the overlying strata, but in a dismembered or mélange-type configuration, the radiolarian-bearing sedimentary matrix should be closely synchronous or younger than any such olistoliths, not older (Cordey, 1998).

3/ The Karpathos ophiolite has a longer age range than previously envisaged, i.e., spanning the Early–Late Cretaceous, more precisely the Aptian–Santonian (from ~125–113 Ma to 84.7 Ma), representing the interval between the radiolarites overlying the ophiolite and the oldest isotopic age in Lastos. In this case, the Xindothio radiolarites should be diachronous. Considering the consistent Early Cretaceous ages from Lastos and Menetes areas (this study), as well as the relatively small volumes of mafic and ultramafic rocks exposed on the island (Figure 2a-c), we do not favour this hypothesis.

4/ Isotopic ages from Lastos have undergone some metamorphic overprint or are affected by argon loss. This is, to us, the most likely cause of the chronological discrepancy, as both

phenomena can cause calculated K-Ar ages to be younger than the true ages of the dated material (McDougall & Harrison, 1999). Similarly, it has been established that some of the youngest Cretan ophiolites underwent such overprinting during the Late Cretaceous (95 Ma; Koepke, Seidel & Kreuzer, 2002). Other authors have also shown that some Cretan isotopic ages record the age of obduction rather than oceanic crust formation (Liati, Gebauer & Fanning, 2004; Stampfli, Champod & Vandelli, 2010). In Turkey, Ar-Ar isotopic ages of the metamorphic soles of the Lycian peridotites are mainly 92−90 Ma (Dilek *et al.* 1999), an age range that is similar to the K-Ar isotopic ages on Karpathos. More recently, U-Pb ages on zircons from the metamorphic sole of the Marmaris ophiolite (Lycian Nappes) have shown that their tectonic emplacement occurred between 100.4 Ma and 93.5 Ma (Cenomanian), suggesting an Early Cretaceous age for the ophiolite and the associated sedimentary rocks (Güngör *et al.* 2018). Unfortunately, previous geochronological studies carried out on Karpathos (Koepke, Kreuzer & Seidel, 1985; Hatzipanagiotou, 1991; Koepke, Seidel & Kreuzer, 2002) did not document the precise locations for the K-Ar samples or indicate whether the magmatic rocks were overlain by sedimentary strata, preventing comparative sampling of sections.

We do not know to what extent the discrepancy between biochronological and geochronological data observed on Karpathos is a localized problem or a larger issue concerning Mesozoic ophiolites. Some isotopic ages established on these ophiolites using K-Ar methods in the 1980s and 1990s probably need to be tested with more up-to-date methods such as Ar-Ar and/or U-Pb, as carried out by and Liati, Gebauer & Fanning (2004) and Smith (2006), who obtained zircon ages on hornblendites and gabbros from Cretan ophiolites, and Parlak et al. (2013) who used hornblendes and zircons from ophiolites of the Tauride belt.

6. Eastern Mediterranean correlations and implications for Neotethys evolution

Tectonic reconstructions of the Eastern Mediterranean region imply the southward migration of the Aegean fore-arc relative to Eurasia since Eocene times, a result of the rollback of subducting African lithosphere (Zachariasse, Van Hinsbergen & Fortuin, 2008; Jolivet *et al.* 2013). Prior to the Paleogene, the paleogeographic evolution of the region has been described by many authors at the scale of the Tethyan Realm (Robertson, 2002; Barrier & Vrielynck, 2008; Menant *et al.* 2016; Barrier *et al.* 2018), but these descriptions lack precision for the islands of the Aegean Sea. Several hypotheses have been proposed for the Karpathos ophiolite: initially, it was correlated with the ophiolites of Crete, both of which were considered the easternmost remnants of the Pindos Nappes of continental Greece and the Peloponnese (Figures 1, 7; Aubouin, Bonneau & Davidson, 1976; van Hinsbergen *et al.* 2005; Papanikolaou, 2013; Ersoy *et al.* 2014; Pantopoulos & Zelilidis, 2014). Other authors have interpreted the Karpathos and Rhodes ophiolites as southwestward extensions of the Lycian Nappes exposed in southwestern Turkey (Figure 1; Robertson, 2002; Koepke, Seidel & Kreuzer, 2002; van Hinsbergen *et al.* 2010). The ophiolites of Karpathos and Rhodes have also been associated with the Late Cretaceous ophiolites of Cyprus, Syria, and Oman (Koepke, Seidel & Kreuzer, 2002), hence as potential remnants of a basin located to the south of Turkey, in a precursor position of the present-day Eastern Mediterranean Basin. In summary, these conflicting interpretations consider the Karpathos ophiolite as an element of the western Northern Neotethys (Pindos Zone), the central Northern Neotethys (Izmir−Ankara−Erzincan suture and Lycian Nappes), or the Southern Neotethys (Cyprus−Syria) (Figure 7).

A geological review of ophiolites exposed in the Aegean fore-arc (Figure 8a) shows that the ophiolite of Karpathos is younger than those of Crete, where K-Ar isotopic ages range from

160 to 140 Ma (Middle−Late Jurassic) (Koepke, Seidel & Kreuzer, 2002; Liati, Gebauer & Fanning, 2004). Notably, the youngest Cretan radiolarites are Late Jurassic in age (Stampfli, Champod & Vandelli, 2010), similar to the Pindos radiolarites of continental Greece (De Wever & Cordey, 1986). Another significant difference is that, on Karpathos, a shallow marine Upper Eocene conglomerate overlies the dismembered ophiolite together with the Mesozoic limestones (Kalilimni Unit) (Figures 2b, 5f), showing that these units were already tectonically assembled while flysch deposition was still continuing in the Pindos Basin farther west.

Our results indicate that the closest chronological and petrological similarities with the ophiolite of Karpathos are found in southwestern Turkey, more specifically within the Lycian Nappes (de Graciansky, 1967; Collins & Robertson, 1997, 2003; Dilek *et al.* 1999; Robertson, 2002). In the Lycian Mélange, Danelian *et al.* (2006) documented Jurassic and Early Cretaceous radiolarian cherts. In the Marmaris ophiolite, the youngest sediments associated with the ophiolite are pre-Cenomanian (Güngör *et al.* 2018).

Many authors have established a link between the Lycian Nappes and the Izmir−Ankara−Erzincan Suture Zone situated to the north of the Menderes metamorphic complex (Figure 8a) (Robertson & Pickett, 2000; Okay *et al.* 2001; Collins & Robertson, 2003; Robertson *et al.* 2004). The Izmir−Ankara−Erzincan Suture Zone is itself considered a remnant of the Northern Neotethyan Ocean (Danelian *et al.* 2006) and records a long history of radiolarite accumulation. In the Central Sakarya Zone, the Dağküplü Mélange includes several slices of mid-ocean ridge metabasalts (MORB-type) that alternate with radiolarites dated to the Middle−Late Jurassic (Bathonian−Tithonian), Early Cretaceous (Hauterivian−Aptian) and early Late Cretaceous (Cenomanian) (Göncüoğlu *et al.* 2000, 2001). Farther east in the Ankara Mélange, blocks of radiolarite associated with gabbro and

pink micritic limestone are dated as Late Triassic, Early Jurassic, Late Jurassic and Early Cretaceous, including Aptian and Albian strata such as on Karpathos (Bragin & Tekin, 1996). As in the Dağküplü Mélange, the youngest radiolarites of the Ankara Mélange are Cenomanian (Bragin & Tekin, 1996). Previous authors noted great similarities in both petrography and trace elements between Karpathos and Rhodes mafic and ultramafic rocks and those of western Turkey, emphasizing the depleted nature of the peridotites and the geochemistry of dykes that are typical of supra-subduction zone ophiolites (Koepke, Seidel & Kreuzer, 2002).

Farther south in the Antalya Complex, MOR-type (mid-ocean ridge) volcanic rocks are overlain by Late Jurassic−Early Cretaceous radiolarian cherts (Robertson & Woodcock, 1982; Yilmaz, 1984; Robertson, 2002), partly coeval with Karpathos radiolarites. However, the Antalya Complex records a distinct geological history and tectonic setting of an oceanic domain located to the south of the Tauride carbonate platform (Figure 7; Barrier & Vrielynck, 2008; Robertson, Parlak & Ustaömer, 2012; Barrier *et al.* 2018).

The ophiolites of Karpathos and Rhodes have also been correlated with the Late Cretaceous ophiolites of Cyprus, Syria, and Oman (Koepke, Seidel & Kreuzer, 2002) and hence interpreted as potential remnants of the Southern Neotethys (Figure 7). However, this hypothesis is not supported by the tectonic interpretations that imply that the emplacement of the Karpathos and Rhodes ophiolites proceeded southward during the closure of a basin located to the north of Turkey (van Hinsbergen *et al.* 2010; Schettino & Turco, 2011).

In summary, the comparison of these various interpretations suggests that the Karpathos ophiolite originated in the central Northern Neotethys (Figure 7; Dilek *et al.* 1999; Robertson, 2002; Barrier & Vrielynck, 2008; Menant *et al.* 2016; Barrier *et al.* 2018) and is linked to the

Lycian Nappes and their root, the Izmir−Ankara−Erzincan Suture Zone. A slight difference lies in the age of the youngest radiolarites between these units: while Karpathos radiolarites are Aptian−Albian (125−100.5 Ma; Cohen *et al.* 2013, updated 2018), the youngest radiolarites of the Lycian Nappes and the Izmir−Ankara−Erzincan Suture Zone are consistently Cenomanian (100.5−93.9 Ma). In addition, the age range represented by the ophiolite is much shorter on Karpathos (late Early Cretaceous). This suggests that the Karpathos ophiolite may be a remnant of a short-lived segment of the Northern Neotethys that was originally located in the westernmost part of the Izmir−Ankara−Erzincan Suture Zone (Figures 7, 8). The convergence and closure of the Northern Neotethys during the Paleogene then led to the thrusting of ophiolite-bearing tectonic slices over the Karpathos parautochthonous carbonate platform, similar to the Lycian Nappes over Rhodes (Figure 8b). Eventually, the southward movement of the Aegean arc during the Neogene distorted the original Paleogene configuration, separating Karpathos farther from the ancient Izmir−Ankara−Erzincan root zone.

7. Conclusions

Our study documents the occurrence of Early Cretaceous radiolarians in sedimentary rocks overlying mafic and ultramafic rocks on the island of Karpathos, with the following implications:

- The older radiolarian assemblage provides a minimum Aptian age (~125−113 Ma) for the ophiolite, while the younger assemblage indicates that the top of the radiolarite-pink limestone subunit is Turonian (~93.9–89.8 Ma). The Aptian and Albian radiolarian ages raise questions regarding the accuracy of a Berriasian age obtained previously from a single calpionellid assemblage in the same subunit.

- The oldest radiolarian ages (late Early Cretaceous) are significantly older than those proposed for the ophiolite using K-Ar geochronology (Late Cretaceous, from 95.3 ± 4.2 Ma to 81.2 ± 1.6 Ma), suggesting that these isotopic ages may have been reset by Late Cretaceous metamorphism, or were affected by argon loss.
- The Karpathos ophiolite should not be associated with the Pindos Nappes or the ophiolites of Cyprus or Syria but rather with the Lycian Nappes and their root located in the Izmir−Ankara−Erzincan Suture Zone, possibly representing the westernmost part of this structure. Consequently, the ophiolite of Karpathos is likely to be a remnant of the Northern Neotethys, not of the Pindos Ocean or the proto-Eastern Mediterranean Basin.
- From an analytical viewpoint, our study suggests that previous K-Ar isotopic ages obtained from the ophiolites of the Mediterranean region should be revised with more recent and accurate methods (Ar-Ar, U-Pb), particularly for geological units that have been affected by syn- or post-emplacement metamorphism and deformation.

Acknowledgements

This study was funded by the Laboratory of Geology of Lyon (LGLTPE, UMR5276) and by the National Research programme Tellus-INTERRVIE of the French CNRS-INSU (Centre National de la Recherche Scientifique – Institut National des Sciences de l'Univers). The authors are grateful to the editor Peter D. Clift as well as Alastair H.F. Robertson and an anonymous reviewer for their very constructive comments concerning previous versions of the manuscript. Geological mapping by John Davidson in the 1970s was a valuable source of information. The authors also wish to thank Jean-Jacques Cornée, Sébastien Joannin (University of Montpellier) and Pierre Moissette (University of Athens) for our discussions on the geology of Karpathos and the Aegean fore-arc.

Declaration of Interest

None

Supplementary Material

Appendix “Pioneering studies on Karpathos” available online at http://journals.cambridge.org/geo

References

AUBOUIN, J. & DERCOURT, J. 1970. Sur la géologie de l’Egée: regard sur le Dodécanèse méridional (Kasos, Karpathos, Rhodes). *Bulletin de la Société Géologique de France* **7** (12), 455–472.

AUBOUIN, J., BONNEAU, M. & DAVIDSON, J. 1976. Contribution à la géologie de l’arc égéen: l’île de Karpathos. *Bulletin de la Société Géologique de France* **7** (18), 385–401.

BARRIER, E. & VRIELYNCK, B. 2008. Palaeotectonic maps of the Middle East. *Commission for the Geological Map of the World, Paris*.

BARRIER, E., VRIELYNCK, B., BROUILLET, J. F. , BRUNET, M. F. 2018. Paleotectonic reconstruction of the Central Tethyan Realm. Tectonono-Sedimentary-Palinspastic maps from Late Permian to Pliocene. *Commission for the Geological Map of the World, Paris.*

BORNOVAS, I. & RONTOGIANNI-TSIABAOU, T. 1983. *Geological map of Greece.* Institute of Geology and Mineral exploration, scale 1:500,000.

456 BRAGIN, N. Y. & TEKIN, U. K. 1996. Age of radiolarian-chert blocks from the Senonian
457 Ophiolitic Mélange (Ankara, Turkey). *The Island Arc* **5**, 114–122.
458
459 CHRISTODOULOU, G. 1960. Geologische und mikropaläontologische untersuchungen auf der
460 insel Karpathos (Dodekanes). *Palaeontographica, Abteilung A*, **115** (1-6), 1–143.
461
462 CHRISTODOULOU, G. 1968. *Karpathos map sheet. Geological map of Greece*. Institute for
463 geology and subsurface research, Athens.
464
465 COHEN, K.M., FINNEY, S.C., GIBBARD, P.L. & FAN, J.-X. 2013 (updated 2018). The ICS
466 International Chronostratigraphic Chart. *Episodes* **36** (3), 199–204.
467
468 COLEMAN, R.G. 1977. *Ophiolites-Ancient Oceanic Lithosphere?* Springer, Berlin, 229 pp.
469
470 COLLINS, A.S., ROBERTSON, A.H.F. 1997. Lycian melange, southwestern Turkey: an emplaced
471 Late Cretaceous accretionary complex. *Geology* **25**, 25– 258.
472
473 COLLINS, A. S. & ROBERTSON, A. H. F. 2003. Kinematic evidence for Late Mesozoic-Miocene
474 emplacement of the Lycian Allochthon over the Western Anatolide Belt. *Geological Journal*
475 **38**, 295– 310.
476
477 CORDEY, F. 1998. Radiolaires des complexes d'accrétion cordillérains. *Geological Survey of*
478 *Canada Bulletin* **509**, 1–210.
479

480 CORDEY, F. & CORNEE, J.-J. 2009. New radiolarian assemblages from La Désirade Island
481 basement complex (Guadeloupe, Lesser Antilles Arc) and Caribbean tectonic implications,
482 *Bulletin de la Société Géologique de France* **180** (5), 399–409.
483
484 CORDEY, F. & KRAUSS, P. 1990. A field technique for identifying and dating radiolaria
485 applied to British Columbia and Yukon. *Geological Survey of Canada Paper* **90-1E**,
486 127–129.
487
488 DANELIAN, T., BONNEAU, M., CADET, J.-P., POISSON, A. & VRIELYNCK, B. 2001.
489 Palaeoceanographic implications of new and revised bio-chronostratigraphic constraints from
490 the Profitis Ilias Unit (Rhodes, Greece). *Bulletin of the Geological Society of Greece* **34** (2),
491 619–625.
492
493 DANELIAN, T., ROBERTSON, A.H.F., COLLINS, A.S. & POISSON, A. 2006. Biochronology of
494 Jurassic and Early Cretaceous radiolarites from the Lycian Mélange (SW Turkey) and
495 implications for the evolution of the Northern Neotethyan ocean. *Geological Society of*
496 *London* **260**, 229–236.
497
498 DAVIDSON-MONETT, J. 1974. Contribution à l'étude géologique de l'arc égéen: l'île de
499 Karpathos (Dodécanèse Méridional, Grèce). Thèse 3ème cycle, University Paris 6, 150 p.
500
501 DE GRACIANSKY, P.C. 1967. Existence d'une nappe ophiolitique à l'extrémité occidentale de la
502 chaîne sud-anatolienne: relations avec les autres unités charriées et avec les terrains
503 autochtones (Province de Muğla, Turquie). *Comptes Rendus Académie Sciences Paris* **264**,
504 2876–2879.
505

DE STEFANI, C., FORSYTH MAJOR, C.J. & BARBEY, W. 1895. Aperçu géologique et paléontologique de l'Ile de Karpathos. In *Karpathos, étude géologique, paléontologique et botanique* (eds. G. Bridel et Cie, Lausanne), 153–164.

DE WEVER, P. & CORDEY, F. 1986. Datation par les radiolaires de la formation des radiolarites s.s. de la série du Pinde-Olonos (Grèce) : Bajocian(?) - Tithonique. *Marine Micropaleontology* **11**, 113–127.

DILEK, Y., & FURNES, H. 2014. Ophiolites and their origins. *Elements* **10**, n° 2, 93-100.

DILEK, Y., THY, P., HACKER, B. & GRUNDVIG, S. 1999. Structure and petrology of Tauride ophiolites and mafic dyke intrusions (Turkey): implications for the Neotethyan ocean. *Geological Society of America Bulletin* **111**, 1192–1216.

ERSOY, E.Y., CEMEN, I., HELVACI, C. & BILLOR, Z. 2014. Tectono-stratigraphy of the Neogene basins in Western Turkey: Implications for tectonic evolution of the Aegean Extended Region. *Tectonophysics* **635**, 33–58.

GARFUNKEL, Z. 2004. Origin of the Eastern Mediterranean basin: a reevaluation. *Tectonophysics* **391**, 11−34.

GÖNCÜOĞLU, M. C., TURHAN, N., SENTÜRK, K., ÖZCAN, A., UYSAL, S. & YALINIZ, M. K. 2000. A geotraverse across northwestern Turkey: tectonic units of the Central Sakarya region and their tectonic evolution. In *Tectonics and Magmatism in Turkey and the Surrounding Area* (eds E. Bozkurt, J. A. Winchester & J. D. A. Piper), pp. 139–161. Geological Society of London, Special Publication no. 173.

GÖNCÜOĞLU, M. C., YALINIZ, M. K., TEKIN, U. K. & TURHAN, N. 2001. Petrology of Late Berriasian-Late Hauterivian and Cenomanian oceanic basalts within the Central Sakarya ophiolitic complex, NW Turkey: constraints for the evolution of the Izmir-Ankara oceanic branch of Neotethys. *Fourth International Turkish Geology Symposium (ITGS IV)*, Cfikfirova University Adana (Turkey), 93.

GORIČAN, S. 1994. Jurassic and Cretaceous radiolarian biostratigraphy and sedimentary evolution of the Budva Zone (Dinarides, Montenegro). *Mémoires de Géologie Lausanne* **18**, 1–176.

GÜNGÖR, T., AKAL, C., ÖZER, S., HASÖZBEK, A., SARI, B., & MERTZ-KRAUS, R. 2018. Kinematics and U-Pb zircon ages of the sole metamorphics of the Marmaris Ophiolite, Lycian Nappes, Southwest Turkey. *International Geology Review*, published online 23 July 2018. doi: 10.1080/00206814.2018.1498029.

GÜRER, D., PLUNDER, A., KIRST, F., CORFU, F., SCHMID, S. M., & VAN HINSBERGEN, D. J. J. 2018. A long-lived Late Cretaceous–Early Eocene extensional province in Anatolia? Structural evidence from the Ivriz Detachment, southern central Turkey. *Earth Planetary Science Letters* **481**, 111–124.

HATZIPANAGIOTOU, K. 1987. Mikrofazies und fauna von karbonatgesteinen der ophiolithischen Melange der südägäischen Inselbrücke. *Newsletters on stratigraphy* **18** (1), 41–50.

HATZIPANAGIOTOU, K. 1988. Einbindung der obersten Einheit von Rhodos und Karpathos (Griechenland) in der alpinischen Ophiolith-Gürtel. *Neues Jahrbuch für Geologie und Paläontologie, Abhandlungen* **176**, 395–442.

HATZIPANAGIOTOU, K. 1991. K-Ar dating of ophiolites from the Rhodes and Karpathos islands, Dodekanese, Greece. *Geologica Balcanica* **21**, 69–76.

JOLIVET, L., RIMMELÉ, G., OBERHÄNSLI, R., GOFFÉ, B. & CANDAN, O. 2004. Correlation of synorogenic tectonic and metamorphic events in the Cyclades, the Lycian Nappes and the Menderes massif, geodynamic implications. *Bulletin de la Société Géologique de France* **175** (3), 217–238.

JOLIVET, L., FACCENNA, C., HUET, B., LABROUSSE, L., LE POURHIET, L., LACOMBE, O., LECOMTE, E., BUROV, E., DENELE, Y., BRUN, J.-P., PHILIPPON, M., PAUL, A., SALAÜN, G., KARABULUT, H., PIROMALLO, C., MONIE, P., GUEYDAN, F., OKAY, A., OBERHÄNSLI, R., POURTEAU, A., AUGIER, R., GADENNE, L. & DRIUSSI, O. 2013. Aegean tectonics: Strain localization, slab tearing and trench retreat. *Tectonophysics* **597–598**, 1–33.

KOEPKE, J., KREUZER, H. & SEIDEL, E. 1985. Ophiolites in the Southern Aegean arc (Crete, Karpathos, Rhodes) - linking the ophiolite belts of the Hellenides and the Taurides. *Ofioliti* **10**, 343–354.

KOEPKE, J., SEIDEL, E. & KREUZER, H. 2002. Ophiolites on the Southern Aegean islands Crete, Karpathos and Rhodes: composition, geochronology and position within the ophiolite belts of the Eastern Mediterranean. *Lithos* **65** (1), 183–203.

LIATI, A., GEBAUER, D. & FANNING, C.M. 2004. The age of ophiolitic rocks of the Hellenides (Vourinos, Pindos, Crete): first U-Pb ion micropobe (SHRIMP) zircon ages. *Chemical Geology* **207**, 171–188.

MCDOUGALL, I., & HARRISON, T.M. 1999. *Geochronology and thermochronology by the 40Ar/39Ar method.* New York, Oxford University Press, 269 pp.

MAFFIONE, M., & VAN HINSBERGEN, D. J. J. 2018. Reconstructing plate boundaries in the Jurassic Neo-Tethys from the East and West Vardar Ophiolites (Greece and Serbia). *Tectonics* **37**, 858–887.

MARTELLI, A. 1916. Appunti geologici sull'Isola di Scarpanto. *Bollettino della Società geologica italiana* **35**, 215–234.

MENANT, A., JOLIVET, L., VRIELYNCK, B. 2016. Kinematic reconstructions and magmatic evolution illuminating crustal and mantle dynamics of the eastern Mediterranean region since the late Cretaceous. *Tectonophysics* **675**, 103–140.

O'DOGHERTY, L. 1994. Biochronology and paleontology of mid-Cretaceous radiolarians from Northern Apennines (Italy) and Betic Cordillera (Spain). *Mémoires de Géologie Lausanne* **21**, 1–413.

O'DOGHERTY, L., CARTER, E.S., DUMITRICA, P., GORICAN, S., DE WEVER, P., BANDINI, N., BAUMGARTNER, P.O. & MATSUOKA, A. 2009. Catalogue of Mesozoic radiolarian genera: Part 2. Jurassic–Cretaceous. *Geodiversitas* **31** (2), 271–356.

609 OKAY, A. I., TANSEL, I. & TÜYSÜZ, O. 2001. Obduction, subduction and collision as reflected
610 in the Upper Cretaceous-Lower Eocene sedimentary record of western Turkey. *Geological*
611 *Magazine* **138**, 117–142.
612
613 PANTOPOULOS, G. & ZELILIDIS, A. 2014. Eocene to early oligocene turbidite sedimentation in
614 the SE Aegean (Karpathos Island, SE Greece): stratigraphy, facies analysis, nannofossil study,
615 and possible hydrocarbon potential. *Turkish Journal of Earth Sciences* **23**, 31–52.
616
617 PAPANIKOLAOU, D. 2013. Tectonostratigraphic models of the Alpine terranes and subduction
618 history of the Hellenides. *Tectonophysics* **595–596**, 1–24.
619
620 PARLAK, O., KARAOGLAN, F., RIZAOGLU, T., KLÖTZLI, U., KOLLER, F. & BILLOR, Z. 2013. U-
621 Pb and $^{40}Ar/^{39}Ar$ Geochronology of the ophiolites and granitoids from the Tauride Belt:
622 Implications for the evolution of the Inner Tauride Suture. *Journal of Geodynamics* **65**, 22–
623 37.
624
625 PESSAGNO, E.A., JR. 1976. Radiolarian zonation and stratigraphy of the Upper Cretaceous
626 portion of the Great Valley Sequence, California Coast Ranges. *Micropaleontology*, Special
627 Publication no. 2, 1–95.
628
629 PESSAGNO, E.A., JR. 1977. Lower Cretaceous radiolarian biostratigraphy of the Great Valley
630 sequence and Franciscan Complex, California Coast Ranges. *Cushman Foundation*
631 *Foraminiferal Research Special Publication* **15**, 1–87.
632
633 PSIMENOS, S., REPPAS, F., MOUZAKI, A., TASSOULA, N. & KODONI, O. 2017. *Karpathos/Kasos*
634 *map sheet 1:30 000*. Terrain Editions, Athens.

ROBERTSON, A.H.F. 2002. Overview of the genesis and emplacement of Mesozoic ophiolites in the Eastern Mediterranean Tethyan region. *Lithos* **65**, 1–67.

ROBERTSON, A.H.F. & WOODCOCK, N.H. 1982. Sedimentary history of the south–western segment of the Mesozoic–Tertiary Antalya continental margin, south–western Turkey. *Eclogae Geologicae Helveticae* **75**, 517–562.

ROBERTSON, A. H. F. & PICKETT, E. A. 2000. Palaeozoic-Early Tertiary Tethyan evolution of mélanges, rift and passive margin units in the Karaburun Peninsula (western Turkey) and Chios Island (Greece). In *Tectonics and Magmatism in Turkey and the Surrounding Area* (eds E. Bozkurt, J. A. Winchester & J. D. A. Piper), pp. 25–42. Geological Society of London, Special Publication no. 173.

ROBERTSON, A. H. F., USTAÖMER, T., PICKETT, E. A., COLLINS, A. S., ANDREW, T. & DIXON, J. E. 2004. Testing models of Late Palaeozoic-Early Mesozoic orogeny in Western Turkey: support for an open-Tethys model. *Journal of the Geological Society* **161**, 201–511.

ROBERTSON, A.H.F., PARLAK, O., USTAÖMER, T. 2012. Overview of the Palaeozoic–Neogene evolution of Neotethys in the Eastern Mediterranean region (southern Turkey, Cyprus, Syria) *Petroleum Geoscience* **18** (4), 381–404.

ROCHE, V., CONAND, C., JOLIVET, L., & AUGIER, R. 2018. Tectonic evolution of Leros Island (Dodecanese, Greece) and correlations between the Aegean Domain and the Menderes Massif. *Journal of the Geological Society* **175**, 836–849.

ROYDEN, L. & FACCENNA, L. 2018. Subduction Orogeny and the Late Cenozoic Evolution of the Mediterranean Arcs. *Annual Review of Earth and Planetary Sciences* **46**, 261–289.

SCHETTINO, A. & TURCO, E. 2011. Tectonic history of the western Tethys since the Late Triassic. *Geological Society of America Bulletin* **123** (1/2), 89–105.

SMITH, A.G. 2006. Tethyan ophiolite emplacement, Africa to Europe motions, and Atlantic spreading. *Geological Society London, Special Publication* **260** (1), 11–34.

STAMPFLI, G., CHAMPOD, E. & VANDELLI, A. 2010. *Tectonostratigraphy and Plate Tectonics of Crete*. Field Guide, University of Lausanne, 64 p.

VAN HINSBERGEN, D.J.J., ZACHARIASSE, W.J., WORTEL, M.J.R. & MEULENKAMP, J.E. 2005. Nappe stacking resulting from subduction of oceanic and continental lithosphere below Greece. *Geology* **33** (4), 325–328.

VAN HINSBERGEN, D.J.J., KAYMAKÇI, N., SPAKMAN, W. & TORSVIK, T.H. 2010. Reconciling the geological history of western Turkey with plate circuits and mantle tomography. *Earth Planetary Science Letters* **297**, 674–686.

VINASSA DE REGNY, P. 1901. Radiolari Cretacei dell'lsola di Karpathos. *Memoria Accademia Scienze Bologna*, serie 5, **9**, 497–512.

YILMAZ, P.O. 1984. Fossil and K–Ar data for the age of the Antalya Complex, S.W. Turkey. In *The Geological Evolution of the Eastern Mediterranean* (eds J.E. Dixon & A.H.F. Robertson), pp. 335– 348. Geological Society London, Special Publication no. 17.

ZACHARIASSE, W.J., VAN HINSBERGEN, D.J.J. & FORTUIN, A.R. 2008. Mass wasting and uplift on Crete and Karpathos (Greece) during the early Pliocene related to beginning of south Aegean left-lateral, strike slip tectonics. *Geological Society of America Bulletin* **120**, 976–993.

Figure captions

Figure 1 (Colour online). Structural map of the southern Aegean region with location of the island of Karpathos (black frame) and the distribution of ophiolites in southern Greece and western Turkey. Compiled from Bornovas & Rontogianni-Tsiabaou (1983), Jolivet *et al.* (2004, 2013), van Hinsbergen *et al.* (2005, 2010), Stampfli, Champod & Vandelli (2010), Ersoy *et al.* (2014), and Gürer *et al.* (2018). The 'eastern' and 'western' ophiolite regions refer to the classification by Robertson (2002). IAE: Izmir−Ankara−Erzincan Suture Zone.

Figure 2. (a) Geological and structural map of Karpathos (modified after Aubouin, Bonneau & Davidson, 1976). (b) Geological map of the Lastos area and location of the radiolarian localities KAL01 (section 'North Lastos road'), KAL02 and KAL03 (section 'Hill 730 m' outlined by a white band). Topography from the Karpathos-Kasos map sheet 1:30 000 (Psimenos *et al.* 2017). Geology based on Christodoulou (1968), Davidson-Monett (1974), Aubouin, Bonneau & Davidson (1976), and personal field observations. (c) Geological map of the Menetes area and location of the radiolarian locality KAM01. Topography from the Karpathos-Kasos map sheet 1:30 000 (Psimenos *et al.* 2017). Geology from the Karpathos map sheet (Christodoulou, 1968).

712 **Figure 3.** (Colour online) (a) Synthetic lithostratigraphic column of the Xindothio Unit
713 succession (modified after Aubouin, Bonneau & Davidson, 1976). Basal radiolarites
714 overlying mafic/ultramafic rocks are presently dated as Aptian (this study) instead of
715 Berriasian (Aubouin, Bonneau & Davidson, 1976). Isotopic ages are from Cohen *et al.* (2013,
716 updated 2018). Dotted lines (left): probable positions of stage boundaries based on
717 biochronological data; red line: thrust fault at the base of mafic/ultramafic rocks; dotted lines
718 (right): boundaries between subunits. (b) Sections in the Lastos and Menetes areas and
719 stratigraphic positions of the radiolarian samples.
720
721 **Figure 4.** (Colour online) Schematic cross-section of the south Lastos area including section
722 'Hill 730 m' and position of samples KAL02 and KAL03 close to the contact with
723 mafic/ultramafic rocks (modified after Aubouin, Bonneau & Davidson, 1976). Note that the
724 Xindothio Unit is structurally situated above the dolomitic limestones of the Kalilimni Unit
725 but underwent Cenozoic extension and normal faulting visible in the southwestern part of the
726 section.
727
728 **Figure 5.** Field views of the studied Karpathos units and localities (see Fig. 2b for locations
729 of photographs). (a) Overview of section 'Hill 730 m' in Lastos (Figs. 2b, 3b, 4) and subunits
730 within the Xindothio Unit (Fig. 3); in the distance towards the west: parautochthonous
731 limestone exposures of Kalilimni Unit; Mount Kalilimni (1215 m) is the highest point on the
732 island. (b) Exposure of serpentinite (white arrows) overlain by the red radiolarite-pink
733 limestone subunit along the north Lastos road (Fig. 2b). White dashed line: contact between
734 ultramafic and sedimentary rocks. White dotted lines: bedding of radiolarite and pink
735 limestone, parallel to the contact between ultramafic and sedimentary rocks. (c) Close-up of
736 the contact between serpentinite and radiolarite (dashed line) along the north Lastos road near
737 locality KAL01 (Fig. 2b). (d) Pink limestone and chert nodules (white arrows) exposed in the

738 middle part of section ‘Hill 730 m’ (total thickness 1 m). (e) Close-up of thick radiolarite beds
739 at the base of section ‘Hill 730 m’ (Lastos, Figs. 2b, 3, 4). (f) Exposure of the Lastos
740 conglomerate (Eocene) displaying a variety of pebbles of radiolarite (white arrows),
741 serpentinite (yellow arrows) and limestones from the underlying Kalilimni and Xindothio
742 units.
743
744 **Figure 6.** Scanning electron microphotographs (SEM) of radiolarian taxa from Lastos (KAL)
745 and Menetes (KAM). For each sample: age and radiolarian assemblage. For each picture:
746 radiolarian taxon, scale length.
747 - Sample KAL03 (Turonian); 1. *Pseudodictyomitra pseudomacrocephala* (SQUINABOL)
748 (210 μm); 2. *Dictyomitra napaensis* PESSAGNO (200 μm); 3. *Dictyomitra montisserei*
749 (SQUINABOL) (220 μm); 4. *Stichomitra communis* (SQUINABOL) (190 μm); 5. *Afens* sp.
750 (200 μm); 6. *Crucella cachensis* PESSAGNO (180 μm); 7. *Patellula verteroensis*
751 (PESSAGNO) (160 μm).
752 - Sample KAL01 (Aptian); 8. *Cenodiscaella sphaeroconus* (RÜST) (200 μm); 9.
753 *Homoeoparonaella* sp. cf. *speciosa* (PARONA) (320 μm); 10. *Crucella messinae*
754 PESSAGNO (240 μm); 11. *Crucella euganea* SQUINABOL (240 μm); 12. *Ultranapora* sp.
755 cf. *durhami* PESSAGNO (140 μm); 13. *Pseudodictyomitra lodogaensis* PESSAGNO (180
756 μm); 14. *Dictyomitra montisserei* (SQUINABOL) (180 μm); 15. *Xitus* sp. aff. *spicularius*
757 (ALIEV) (210 μm); 16. *Archaeodictyomitra gracilis* (SQUINABOL) (200 μm); 17.
758 *Archaeodictyomitra gracilis* (SQUINABOL) (180 μm); 18. *Hiscocapsa asseni* (TAN) (120
759 μm); 19. *Hiscocapsa grutterinki* (TAN) (150 μm).
760 - Sample KAL02 (early−middle Albian); 20. *Obeliscoites* sp. cf. *perspicuus* (SQUINABOL)
761 (180 μm); 21. *Xitus spicularius* (ALIEV) (190 μm); 22. *Dactyliosphaera lepta* FOREMAN
762 (200 μm); 23. *Dactyliosphaera* sp. cf. *lepta* FOREMAN (200 μm); 24. *Mesosaturnalis* sp.

(190 μm); 25. *Hexapyramis* sp. cf. *precedis* JUD (190 μm); 26. *Cyclastrum satoi* (TUMANDA) (180 μm).

- Sample KAM01 (middle Albian); 27. *Cenodiscaella tuberculatum* (DUMITRICA) (160 μm); 28. *Staurosphaeretta* sp. (130 μm); 29. *Thanarla brouweri* (TAN) (120 μm); 30. *Archaeospondoprumum renaensis* PESSAGNO (180 μm); 31. *Distylocapsa micropora* (SQUINABOL) (180 μm).

Figure 7. Schematic paleogeographic map of western Neotethyan basins in the Cretaceous. Compiled from Barrier & Vrielynck (2008), Robertson, Parlak & Ustaömer (2012), Menant *et al.* (2016), Barrier *et al.* (2018), Maffione & van Hinsbergen (2018). Star: hypothetical position of Karpathos ophiolite prior to obduction. Note that the ophiolites and the tectonic nappes depicted in the diagram have been emplaced diachronously: they just indicate the initial locations and relationships to the surrounding oceanic basins.

Figure 8. (a) Map of the Aegean region prior to the complete southward migration of the Aegean fore-arc during the Neogene (modified after Garfunkel, 2004). The map shows the position of the ophiolites and the extensions of the Pindos and Lycian nappes, which have been proposed as potential sources for the ophiolite-bearing units of Crete, Karpathos, and Rhodes. A-B: cross-section shown in (b). Isotopic ages, Crete: Koepke, Seidel & Kreuzer (2002); Liati, Gebauer & Fanning (2004). Karpathos and Rhodes: Koepke, Seidel & Kreuzer (2002). Southwestern Turkey: Dilek *et al.* (1999); Güngör *et al.* (2018) (see references for age ranges, error margins and local distribution). Age of radiolarites, Crete: Stampfli, Champod & Vandelli (2010); Turkey: Danelian *et al.* (2006); Karpathos: this study. IAE: Izmir−Ankara−Erzincan Suture Zone. (b) Cross-section A-B (Fig. 8a) from the Eastern Mediterranean Basin to the Izmir−Ankara−Erzincan Suture Zone (modified after van

788 Hinsbergen *et al.* 2010), illustrating the southward thrusting of the Lycian Nappes and related
789 ophiolites over Rhodes and Karpathos.
790

791 Table 1. K-Ar isotopic ages in the Lastos and Menetes areas (Koepke, Seidel & Kreuzer,

792 2002) and correlation with geological stages (Cohen *et al.* 2013, updated 2018).

793
794

	K-Ar age (Ma)	Error (Ma)	Lower limit	Upper limit
Lastos	83.1	± 1.6	84.7 middle Santonian	81.5 early Campanian
	81.2	± 1.6	82.8 early Campanian	79.6 middle Campanian
Menetes	91.9	± 3.5	95.4 late Cenomanian	88.4 early Coniacian
	95.3	± 4.2	99.5 early Cenomanian	91.1 middle Turonian
	88.8	± 5	93.8 basal Turonian	83.8 late Santonian

795

796 Table 2. Geographic coordinates of radiolarian samples from Karpathos.

797

Lastos	KAL01	N 35° 34' 51.90"	E 27° 08' 35.96"
	KAL02	N 35° 34' 16.08"	E 27° 08' 26.14"
	KAL03	N 35° 34' 20.66"	E 27° 08' 30.57"
Menetes	KAM01	N 35° 29' 28.59"	E 27° 09' 3.84"

798

799 Table 3. Radiolarian taxa and assemblages from Karpathos.
800
801

Taxa	KAL01	KAL02	KAL03	KAM01
Afens sp.			x	
Alievium sp.		x		
Alievum sp. cf. *superbum* (SQUINABOL)			x	
Archaeodictyomitra gracilis (SQUINABOL)	x			
Archaeospongoprunum renaensis PESSAGNO				x
Archaeospongoprunum sp.			x	
Cenodiscaella sphaeroconus (RÜST)	x			
Cenodiscaella tuberculatum (DUMITRICA)				x
Crucella cachensis PESSAGNO			x	
Crucella euganea SQUINABOL	x			
Crucella messinae PESSAGNO	x	x		
Cyclastrum satoi (TUMANDA)		x		
Dactyliosphaera lepta FOREMAN		x		
Dictyomitra montisserei (SQUINABOL)	x		x	
Dictyomitra napaensis PESSAGNO			x	
Distylocapsa micropora SQUINABOL				x
Falsocromyodrymus sp.			x	
Hexapyramis sp. cf. *precedis* JUD		x		
Hiscocapsa asseni (TAN)	x			
Hiscocapsa grutterinki (TAN)	x			
Homoeoparonaella sp. cf. *speciosa* (PARONA)	x			
Mesosaturnalis levis (DONOFRIO & MOSTLER)		x		
Mesosaturnalis sp.	x			
Obeliscoites sp. cf. *perspicuus* (SQUINABOL)		x		
Paronaella sp.	x			
Patellula verteroensis (PESSAGNO)			x	
Pseudocrucella sp. aff. *kubischa* EMPSON-MORIN	x			
Pseudodictyomitra lodogaensis PESSAGNO	x			x
Pseudodictyomitra pseudomacrocephala (SQUINABOL)			x	
Pseudoeucyrtis (?) *fusus* JUD	x			
Staurosphaeretta sp.				x
Stichomitra communis (SQUINABOL)	x		x	
Thanarla brouweri (TAN)				x
Triactoma sp.				x
Ultranapora sp. cf. *durhami* PESSAGNO	x			
Xitus sp. aff. *spicularius* (ALIEV)	x			
Xitus spicularius (ALIEV)		x		

802

Figure 1 (Colour online). Structural map of the southern Aegean region with location of the island of Karpathos (black frame) and the distribution of ophiolites in southern Greece and western Turkey. Compiled from Bornovas & Rontogianni-Tsiabaou (1983), Jolivet *et al.* (2004, 2013), van Hinsbergen *et al.* (2005, 2010), Stampfli, Champod & Vandelli (2010), Ersoy *et al.* (2014), and Gürer *et al.* (2018). The 'eastern' and 'western' ophiolite regions refer to the classification by Robertson (2002). IAE: Izmir–Ankara–Erzincan Suture Zone.

167x114mm (600 x 600 DPI)

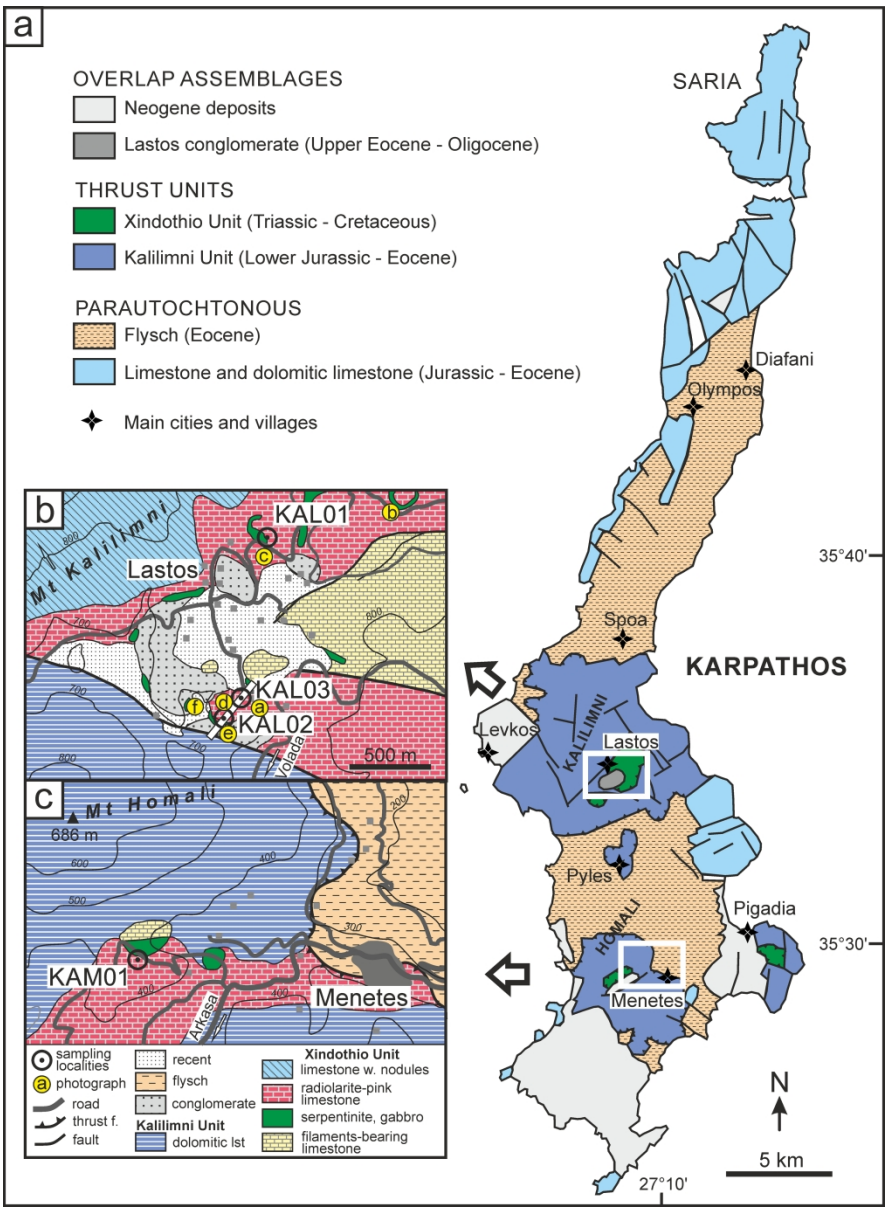

Figure 2. (a) Geological and structural map of Karpathos (modified after Aubouin, Bonneau & Davidson, 1976). (b) Geological map of the Lastos area and location of the radiolarian localities KAL01 (section 'North Lastos road'), KAL02 and KAL03 (section 'Hill 730 m' outlined by a white band). Topography from the Karpathos-Kasos map sheet 1:30 000 (Psimenos *et al.* 2017). Geology based on Christodoulou (1968), Davidson-Monett (1974), Aubouin, Bonneau & Davidson (1976), and personal field observations. (c) Geological map of the Menetes area and location of the radiolarian locality KAM01. Topography from the Karpathos-Kasos map sheet 1:30 000 (Psimenos *et al.* 2017). Geology from the Karpathos map sheet (Christodoulou, 1968).

165x225mm (600 x 600 DPI)

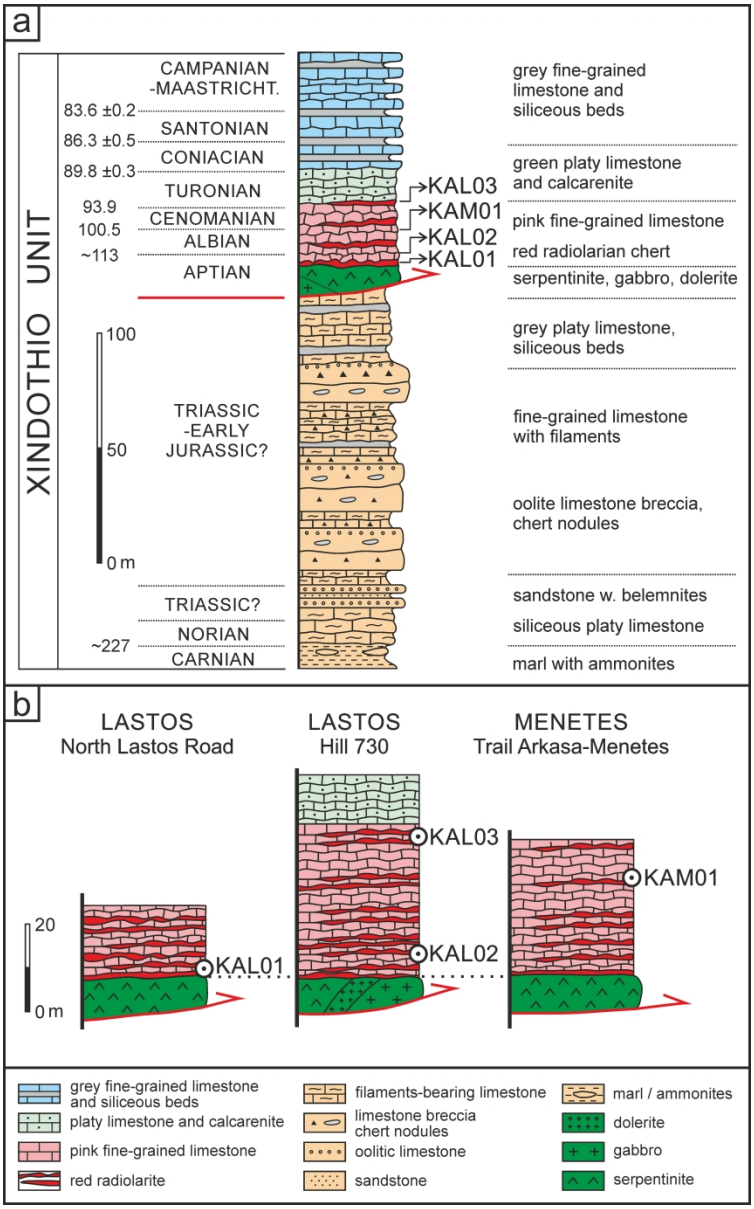

Figure 3. (Colour online) (a) Synthetic lithostratigraphic column of the Xindothio Unit succession (modified after Aubouin, Bonneau & Davidson, 1976). Basal radiolarites overlying mafic/ultramafic rocks are presently dated as Aptian (this study) instead of Berriasian (Aubouin, Bonneau & Davidson, 1976). Isotopic ages are from Cohen *et al.* (2013, updated 2018). Dotted lines (left): probable positions of stage boundaries based on biochronological data; red line: thrust fault at the base of mafic/ultramafic rocks; dotted lines (right): boundaries between subunits. (b) Sections in the Lastos and Menetes areas and stratigraphic positions of the radiolarian samples.

144x231mm (600 x 600 DPI)

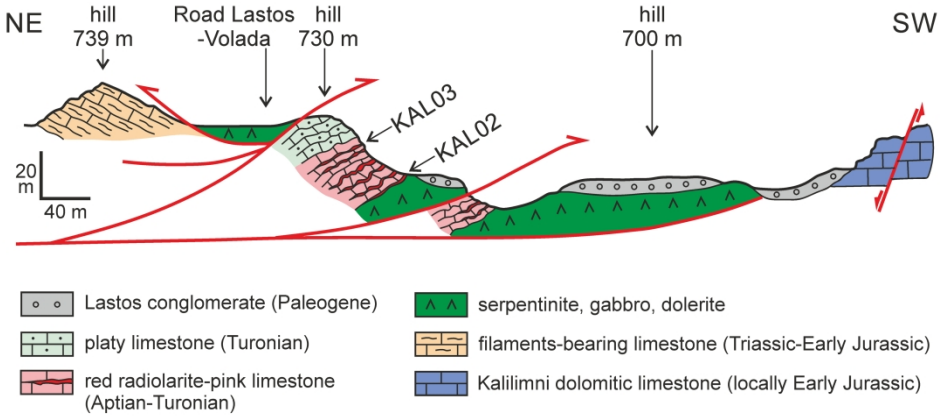

Figure 4. (Colour online) Schematic cross-section of the south Lastos area including section 'Hill 730 m' and position of samples KAL02 and KAL03 close to the contact with mafic/ultramafic rocks (modified after Aubouin, Bonneau & Davidson, 1976). Note that the Xindothio Unit is structurally situated above the dolomitic limestones of the Kalilimni Unit but underwent Cenozoic extension and normal faulting visible in the southwestern part of the section.

165x75mm (600 x 600 DPI)

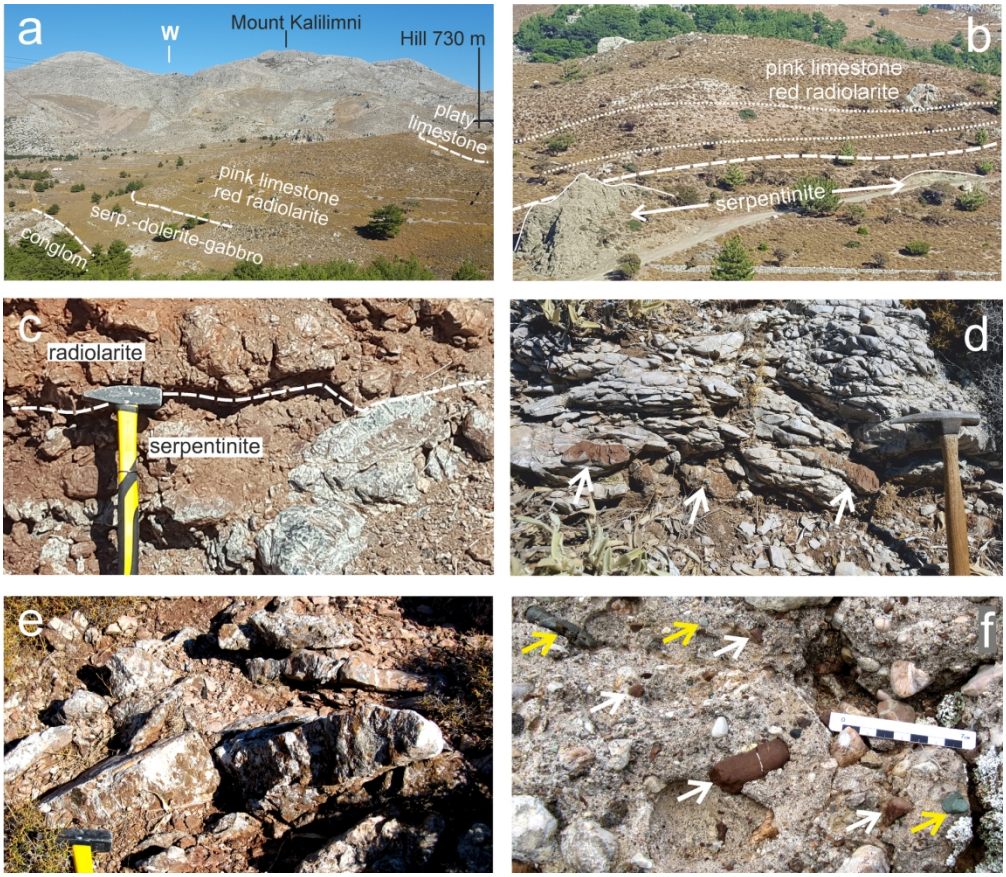

Figure 5. Field views of the studied Karpathos units and localities (see Fig. 2b for locations of photographs). (a) Overview of section 'Hill 730 m' in Lastos (Figs. 2b, 3b, 4) and subunits within the Xindothio Unit (Fig. 3); in the distance towards the west: parautochthonous limestone exposures of Kalilimni Unit; Mount Kalilimni (1215 m) is the highest point on the island. (b) Exposure of serpentinite (white arrows) overlain by the red radiolarite-pink limestone subunit along the north Lastos road (Fig. 2b). White dashed line: contact between ultramafic and sedimentary rocks. White dotted lines: bedding of radiolarite and pink limestone, parallel to the contact between ultramafic and sedimentary rocks. (c) Close-up of the contact between serpentinite and radiolarite (dashed line) along the north Lastos road near locality KAL01 (Fig. 2b). (d) Pink limestone and chert nodules (white arrows) exposed in the middle part of section 'Hill 730 m' (total thickness 1 m). (e) Close-up of thick radiolarite beds at the base of section 'Hill 730 m' (Lastos, Figs. 2b, 3, 4). (f) Exposure of the Lastos conglomerate (Eocene) displaying a variety of pebbles of radiolarite (white arrows), serpentinite (yellow arrows) and limestones from the underlying Kalilimni and Xindothio units.

165x143mm (300 x 300 DPI)

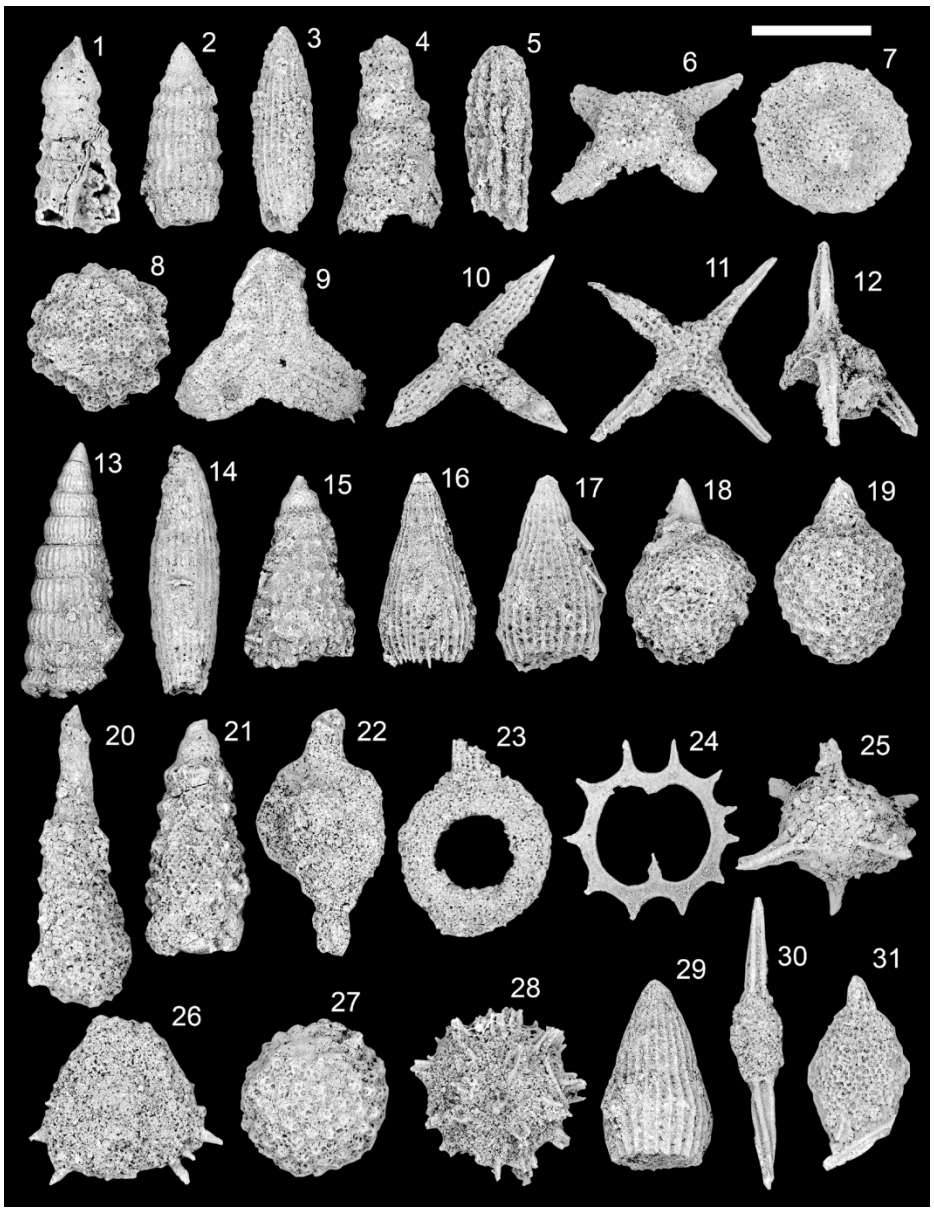

Figure 6. Scanning electron microphotographs (SEM) of radiolarian taxa from Lastos (KAL) and Menetes (KAM). For each sample: age and radiolarian assemblage. For each picture: radiolarian taxon, scale length. Sample KAL03 (Turonian): 1. *Pseudodictyomitra pseudomacrocephala* (SQUINABOL) (210 μm); 2. *Dictyomitra napaensis* PESSAGNO (200 μm); 3. *Dictyomitra montisserei* (SQUINABOL) (220 μm); 4. *Stichomitra communis* (SQUINABOL) (190 μm); 5. *Afens* sp. (200 μm); 6. *Crucella cachensis* PESSAGNO (180 μm); 7. *Patellula verteroensis* (PESSAGNO) (160 μm). Sample KAL01 (Aptian): 8. *Cenodiscaella sphaeroconus* (RÜST) (200 μm); 9. *Homoeoparonaella* sp. cf. *speciosa* (PARONA) (320 μm); 10. *Crucella messinae* PESSAGNO (240 μm); 11. *Crucella euganea* SQUINABOL (240 μm); 12. *Ultranapora* sp. cf. *durhami* PESSAGNO (140 μm); 13. *Pseudodictyomitra lodogaensis* PESSAGNO (180 μm); 14. *Dictyomitra montisserei* (SQUINABOL) (180 μm); 15. *Xitus* sp. aff. *spicularius* (ALIEV) (210 μm); 16. *Archaeodictyomitra gracilis* (SQUINABOL) (200 μm); 17. *Archaeodictyomitra gracilis* (SQUINABOL) (180 μm); 18. *Hiscocapsa asseni* (TAN) (120 μm); 19. *Hiscocapsa grutterinki* (TAN) (150 μm). Sample KAL02 (early–middle Albian): 20. *Obeliscoites* sp. cf. *perspicuus* (SQUINABOL) (180 μm); 21. *Xitus spicularius* (ALIEV) (190 μm); 22. *Dactyliosphaera lepta* FOREMAN (200 μm); 23. *Dactyliosphaera* sp. cf. *lepta* FOREMAN (200 μm); 24.

Mesosaturnalis sp. (190 µm); 25. *Hexapyramis* sp. cf. *precedis* JUD (190 µm); 26. *Cyclastrum satoi* (TUMANDA) (180 µm). Sample KAM01 (middle Albian): 27. *Cenodiscaella tuberculatum* (DUMITRICA) (160 µm); 28. *Staurosphaeretta* sp. (130 µm); 29. *Thanarla brouweri* (TAN) (120 µm); 30. *Archaeospondoprumum renaensis* PESSAGNO (180 µm); 31. *Distylocapsa micropora* (SQUINABOL) (180 µm).

167x217mm (300 x 300 DPI)

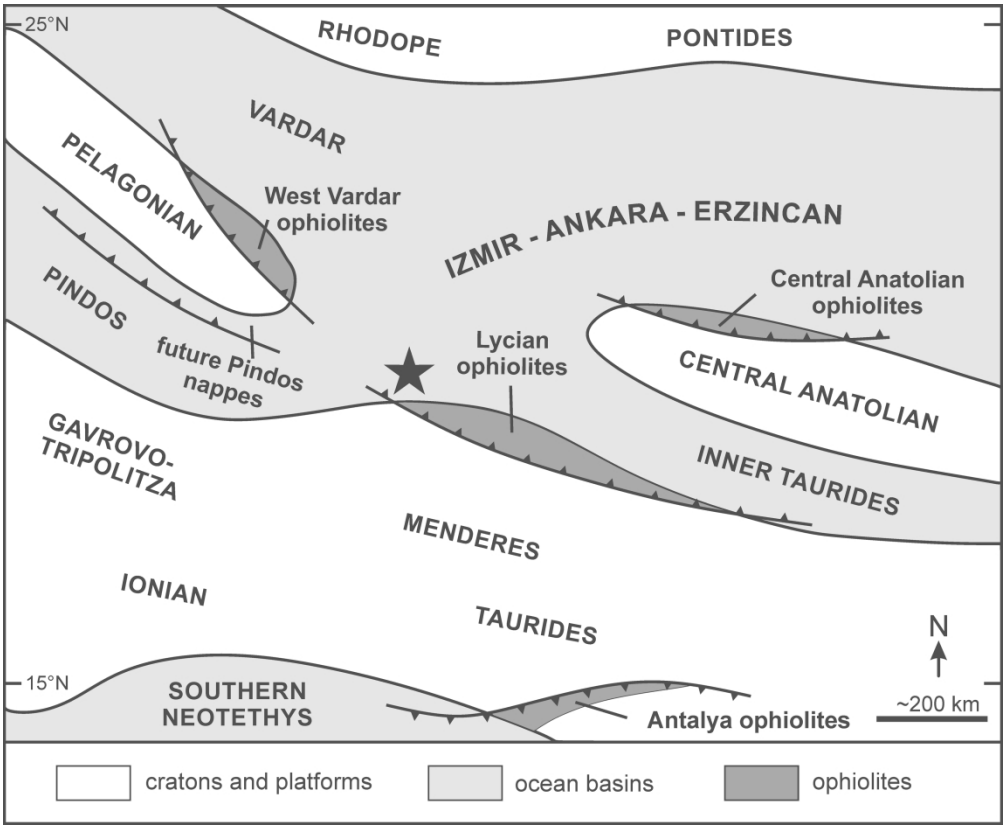

Figure 7. Schematic paleogeographic map of western Neotethyan basins in the Cretaceous. Compiled from Barrier & Vrielynck (2008), Robertson, Parlak & Ustaömer (2012), Menant *et al.* (2016), Barrier *et al.* (2018), Maffione & van Hinsbergen (2018). Star: hypothetical position of Karpathos ophiolite prior to obduction. Note that the ophiolites and the tectonic nappes depicted in the diagram have been emplaced diachronously: they just indicate the initial locations and relationships to the surrounding oceanic basins.

149x123mm (600 x 600 DPI)

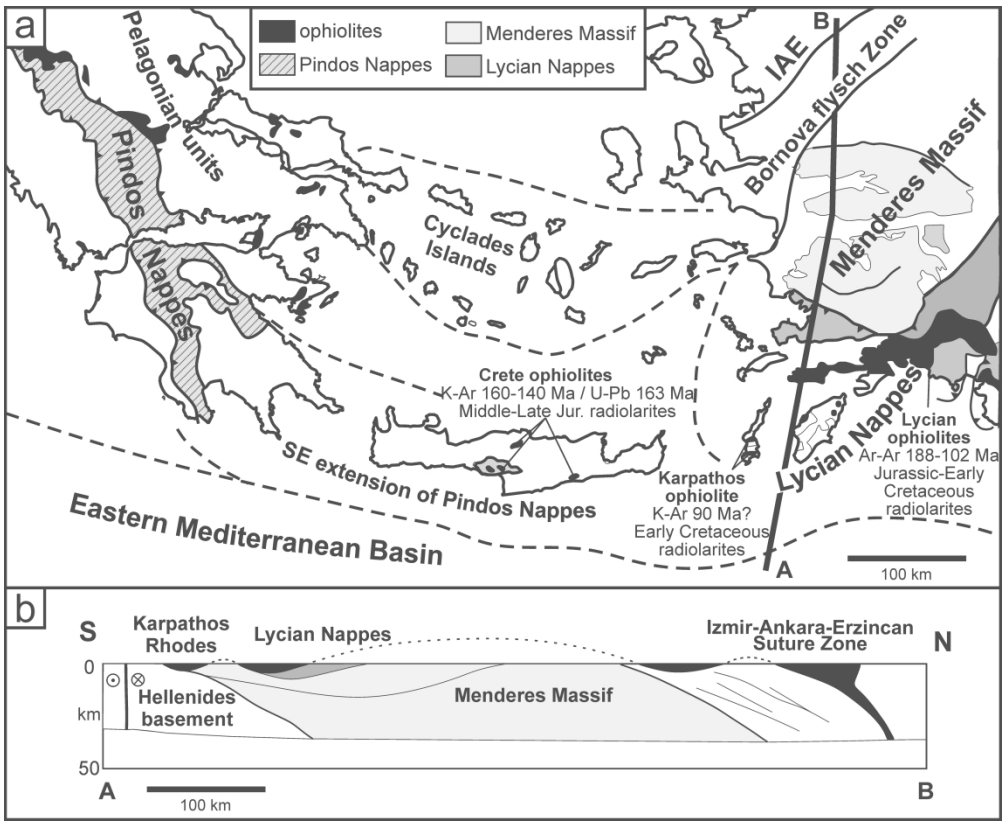

Figure 8. (a) Map of the Aegean region prior to the complete southward migration of the Aegean fore-arc during the Neogene (modified after Garfunkel, 2004). The map shows the position of the ophiolites and the extensions of the Pindos and Lycian nappes, which have been proposed as potential sources for the ophiolite-bearing units of Crete, Karpathos, and Rhodes. A-B: cross-section shown in (b). Isotopic ages, Crete: Koepke, Seidel & Kreuzer (2002); Liati, Gebauer & Fanning (2004). Karpathos and Rhodes: Koepke, Seidel & Kreuzer (2002). Southwestern Turkey: Dilek *et al.* (1999); Güngör *et al.* (2018) (see references for age ranges, error margins and local distribution). Age of radiolarites, Crete: Stampfli, Champod & Vandelli (2010); Turkey: Danelian *et al.* (2006); Karpathos: this study. IAE: Izmir−Ankara−Erzincan Suture Zone. (b) Cross-section A-B (Fig. 8a) from the Eastern Mediterranean Basin to the Izmir−Ankara−Erzincan Suture Zone (modified after van Hinsbergen *et al.* 2010), illustrating the southward thrusting of the Lycian Nappes and related ophiolites over Rhodes and Karpathos.

167x136mm (600 x 600 DPI)